Anderson localization of thermal phonons leads to a thermal conductivity maximum

Jonathan Mendoza and Gang Chen*

Department of Mechanical Engineering, Massachusetts Institute of Technology, Cambridge, Massachusetts, 02139, USA

Abstract

Our elastic model of ErAs disordered GaAs/AlAs superlattices exhibits a local thermal conductivity maximum as a function of length due to exponentially suppressed Anderson-localized phonons. By analyzing the sample-to-sample fluctuations in the dimensionless conductance, g, the transition from diffusive to localized transport is identified as the crossover from the multi-channel to single-channel transport regime $g \approx 1$. Single parameter scaling is shown to hold in this crossover regime through the universality of the probability distribution of g that is independent of system size and disorder strength.

Investigations of phonon transport have invalidated Fourier's law at the nanoscale [1–3]. As the length scale becomes smaller than the phonon mean free path, phonons ballistically propagate across the sample with a probability of order unity. If the essential heat carrying phonon modes, populated at a given temperature, are ballistic, the thermal conductivity of the material should scale linearly with the length of 3-d systems. This coherent transport regime was verified in GaAs/AlAs superlattices (SLs) at temperatures up to 150K [4]. In this coherent transport regime, the introduction of disorder can greatly impact phonon transport through elastic scattering.

In his seminal work, Anderson predicted that sufficiently strong disorder could localize waves and completely suppress coherent transport [5]. Although originally intended for electron transport described by the tight-binding Schrödinger equation, the essential concept has been applied to classical electromagnetic and acoustic wave equations owing to the fact that Anderson localization stems from interference [6–10]. In contrast to photonic materials, which can be essentially non-interacting, phononic systems which describe thermal transport require low temperatures to mitigate phase breaking phonon-phonon interactions. Unfortunately, since Rayleigh scattering scales as $\sim\omega^4$, significant localization can only exist at higher frequencies; consequently, the low temperatures required for coherent transport may not populate these high frequency localized phonons to a significant enough degree to influence thermal transport. This difficulty is demonstrated in the numerical study of isotope-disordered nanotubes [11].

The problems with observing localization in three dimensions are further compounded by a critical level of disorder required for strong localization [12]. Owing to the work of John, who suggested that disordered 3-d photonic crystals should localize light near band edge frequencies [8], we were motivated to find an appropriate analogy

* To whom correspondence should be addressed: gchen2@mit.edu

for phononic crystals. Recently, thermal measurements have demonstrated decreasing thermal conductivity as a function of length in GaAs/AlAs superlattices with embedded ErAs nanoparticles [13]. Anderson localization is the implied mechanism for this trend since the exponentially suppressed phonon conductance outweighs the linear scaling of ballistic modes.

In this work, we report numerical results obtained from the non-equilibrium Green function (NEGF) [14,15] and Landauer-Büttiker transport formalism [16] for GaAs/AlAs superlattices with ErAs nanoparticles. The primary finding is the transition from ballistic to localized transport as temperature and system size are varied. At very low temperatures (~1K), the populated modes are ballistic; consequently, the thermal conductivity exhibits linear size dependence. As the temperature increases, localized modes become populated, resulting in a decreasing thermal conductivity with increasing length. The calculated localization lengths for normal incidence phonons further corroborate the importance of phonon localization at intermediate frequencies. Additionally, the statistics of the dimensionless conductance [17] can be used to infer the diffusive or localized behavior of a given phonon mode [18]. We found that at length scales corresponding to the transition from diffusive to localized transport, the probability distribution of the dimensionless conductance, g, develops non-analytic behavior around $g \approx 1$ [19,20], suggesting transport governed by a single-channel [21–23].

The coherent phonon transport problem in this work concerns the transmission of phonons, whose spectrum is governed by ordered, semi-infinite GaAs leads, through disordered GaAs/AlAs superlattices (Fig. 1). The quasi 1-D geometry has a transverse area of $3a \times 3a$ = 1.7 nm × 1.7 nm and a period length of $10a$, where the lattice constant a = 5.66Å is chosen to be an average of the lattice constants of GaAs and AlAs. Periodic boundary conditions in the transverse direction are imposed; consequently, a k-mesh of 10×10 ensures converged transmission of thermal phonons. The SL interatomic force constants (IFCs), obtained through Density Functional Perturbation Theory [24], are an average of bulk GaAs and AlAs IFCs. Disorder is introduced by perturbing the mass terms of the dynamical matrix, leaving the IFCs unaffected. Interfacial roughness is implemented by randomizing the Ga and Al atoms within one unit cell of the interface. ErAs particles with diameter $2a$ are generated randomly at the interfaces with area concentrations of integer multiples of 2.38%, which corresponds to ~1 nanoparticle every 10 periods. The thermal conductivity of a disordered SL of length L coupled to GaAs leads, depicted in Fig. 1, can be written as $\kappa = \frac{L}{A}\int_0^\infty \frac{\hbar\omega}{2\pi}\frac{\partial f(\omega,T)}{\partial T}\langle g(\omega)\rangle d\omega$, where A is the transverse area, ω is the phonon frequency, f is the Bose-Einstein distribution, T is the temperature, g is the dimensionless conductance after averaging over the first Brillouin zone, and $\langle ... \rangle$ corresponds to a configuration averaged quantity. The dimensionless conductance can be expressed as $g(\omega) = Tr[\Gamma_L G \Gamma_R G^\dagger]$. $\Gamma_{L,R} = i(\Sigma_{L,R} - \Sigma_{L,R}^\dagger)$ corresponds to the absorption rate of the leads, $\Sigma_{L,R}$ is the self-energy due to the interaction of the disordered region with the leads, and G is the Green function of the disordered region. The self-energies are computed through a real-space decimation technique [25], while the Green function matrix elements connecting the two ends are recursively solved by the Dyson equation [26].

At low temperatures, when inelastic scattering is negligible, disorder introduces two length scales, the elastic mean free path, l_{mfp}, and the localization length, ξ. At

system sizes $L < l_{mfp}$, the ballistic regime is characterized by a dimensionless conductance independent of system size, i.e. phonons propagate across the sample with unity probability. When l_{mfp} and ξ are well separated, the diffusive regime, $l_{mfp} \ll L \ll \xi$, exhibits power law decay $g(\omega) \propto L^{-1}$. As the length scale reaches deep into the localized regime, $\xi \ll L$, the dimensionless conductance behaves as $g(\omega) \propto e^{-\frac{L}{\xi}}$. The dimensionless conductance of Fig. 2(a) shows evidence of phonon transport in all three regimes. At frequencies below ~0.5 THz the dimensionless conductance is independent of system sizes up to 100 period lengths (~560 nm). Above this frequency threshold, l_{mfp} becomes the relevant length scale. At a phonon frequency of ~1.5 THz, the conductance transitions from power law to exponential decay, signifying the onset of significant phonon localization.

To put the frequency intervals associated with ballistic, diffusive, and localized transport on a more quantitative footing, l_{mfp} and ξ are calculated for frequencies up to 6 THz. From the relationship $\langle g(\omega) \rangle = N(\omega)(1 + \frac{L}{l_{mfp}})^{-1}$ [27], a linear fit to $\frac{L}{l_{mfp}} = \frac{N(\omega)}{\langle g(\omega) \rangle} - 1$ can be used to obtain l_{mfp}, where $N(\omega)$ is the number of phonon modes transmitted in the superlattice without ErAs and interface roughness. In a similar fashion, $\xi = \frac{-L}{\langle \ln\, g(\omega) \rangle}$ is calculated from the configuration average of 1680 nm systems. Additionally, under the assumption of weak isotropic scattering, the Thouless relationship, $\xi_{thouless} \propto N(\omega) l_{mfp}$, provides a qualitative estimate of the length scale over which diffusive transport occurs in quasi 1-D geometries. Fig. 2(b) illustrates the frequency dependence of l_{mfp}, ξ, and the localization length obtained from the Thouless relationship. The frequencies 0.5 THz and 1.5 THz correspond to the regime where l_{mfp} and ξ is on the order of ~10^2 nm, respectively. Although l_{mfp} and ξ are proportional to each other, the Thouless relationship $\xi_{thouless} \approx 2(N(\omega) + 1) l_{mfp}$ [28,29] primarily holds for frequencies below 1.5 THz. Additionally, the Thouless relationship fails when the mean free path drops near band edges. The strong disorder ($\frac{m_{Er}}{m_{Al}} = 6.2$) and anisotropy stemming from the superlattice structure are potential causes for the failure of the Thouless relationship at higher frequencies [30]. Furthermore, since GaAs reservoirs are coupled to the superlattice, some phonon modes in the ordered system will still be scattered due to contact resistance, i.e. $N(\omega)$ should be calculated using ordered GaAs/AlAs superlattice reservoirs. The most notable feature of l_{mfp} and ξ is the strong departure from Rayleigh behavior at 1.5 THz when both values suddenly drop two orders of magnitude. Since 1.5 THz corresponds to the fifth band edge in the zone-folded Brillouin zone representation, the low group velocities leads to resonant scattering [8,31,32]. Beyond 1.5 THz, l_{mfp} hovers around one period length. This is a sensible value since a 23.8% area density corresponds to, on average, one nanoparticle every period in our simulated domain.

Unlike the conduction problem in electronic systems, where carriers within $k_B T$ of the Fermi energy primarily contribute to transport, phonon thermal conduction includes both sub-THz and THz contributions. Due to this broadband nature, the conduction within our simulated systems will consist of a combination of ballistic, diffusive, and localized modes. If the localized contribution to thermal conductivity is too small, as in

the case of Savic et. al [11], the effects of interference merely corrects the $\lim_{L\to\infty}\kappa(L)$ behavior. In other words, $\kappa(L)$ will still be monotonically increasing with increasing length (in the absence of inelastic scattering) since the growing contributions from ballistic modes outweigh the decreasing contributions from localized modes. As localized transport becomes more significant, $\kappa(L)$ will display a local maximum as a function of length then asymptote to a lower bulk value as the localized modes become completely suppressed. Observing the latter trend in experiments [13] is a much stronger implication of Anderson localization because small corrections to the bulk thermal conductivity can be attributed to underestimated long-range disorder or anharmonicity.

The difficulty in observing localized phonon contributions to thermal transport stems from the fine-tuning of the temperature. At temperatures below this threshold, the populated modes will be predominantly of the ballistic and diffusive type, resulting in conventional length dependence. When the temperature is too high, the anharmonic mean free path, $l_{anh} \propto T^{-1}$, approaches ξ, leading to classical Ohmic behavior as interference effects become negligible. To validate our phase-preserving transport models, we compare our system sizes and localization lengths to the anharmonic mean free paths computed for ordered GaAs/AlAs superlattices in [13]. Calculations performed up to 100K ensure $l_{anh}(\omega)$ is greater than L and ξ up to phonon frequencies of 4 THz, which constitutes 91% and 99.9% of the accumulated thermal conductivity for $L = 140$nm and $L = 560$ nm, respectively.

Calculations performed at 1K depict linear scaling of the thermal conductivity for lengths up to 560 nm for various levels of nanoparticle densities and justify the transition from ballistic to diffusive transport as T increases. $\kappa(L)$, shown in Fig. 3, is calculated for T = 10K and T = 100K and ErAs interfacial area density of 2.38% and 23.8%. At 10K, both levels of disorder obey similar scaling behaviors, implying transport governed predominantly by ballistic and diffusive phonons. Here, the diffusive scattering is caused by momentum randomization due to elastic scattering, since phase breaking anharmonic processes have much larger mean free paths. At 100K there is a clear departure in the behavior of the low nanoparticle concentration and the high nanoparticle concentration superlattices. While the 2.38% sample monotonically increases to a bulk thermal conductivity, the 23.8% sample exhibits a maximum thermal conductivity at L = 112 nm. The ratio of the maximum thermal conductivity to the value calculated for L = 560 nm is ~2.1. Although the simulations are limited to small transverse dimensions, increasing the size of the ErAs nanoparticles should enhance this ratio. Larger nanoparticles should be able to reduce the frequency where l_{mfp} saturates to the approximate lower bound of L_{period}, thus enabling significant localization for even lower frequency phonons.

It is instructive to consider how this ratio should change if one were to include anharmonicity. As the system transitions from diffusive transport to localized transport as T increases, the ratio should grow from unity to some maximum value. As T is increased further, phase breaking interactions should delocalize phonons, decreasing this ratio back to unity [33]. The temperature associated with the onset of a local thermal conductivity maximum is determined by the calculation of $\kappa(T)$ for different values of L, as shown in Fig. 4. At ~18K, anomalous length dependence causes the 560 nm superlattice thermal conductivity to become smaller than the shorter superlattices. As the temperature increases to ~40K, the 560 nm superlattice becomes as thermally insulating as the 11.2 nm superlattice.

Up until this point, our calculations were primarily concerned with configurationally averaged values of g or $\ln(g)$. While these sorts of averaging procedures provide insight into ergodic systems, strongly localized waves are not exposed to the multitude of disorder configurations that extended waves interact with over the same period of time. Additionally, the transition from diffusive to localized transport, for a given phonon frequency, can be made more explicit by analyzing the statistics of the dimensionless conductance. In the diffusive regime, the probability distribution of the dimensionless conductance, $P[g(\omega)]$, is Gaussian with a variance of order unity [18]. Physically this universal conductance fluctuation [34] corresponds to interference opening or closing a single conductance channel. The connection to quantized conductance channels can be made complete by identifying $g = Tr[\Gamma_L G \Gamma_R G^\dagger]$ with the dimensionless conductance $G = 2Tr[tt^\dagger]$, where t is the transmission coefficient matrix which couples ingoing and outgoing waves [17,35]. The Hermitian matrices being traced over can be diagonalized; consequently, the trace can be written as $g = \sum_i \tau_i$, where τ_i are the transmission eigenvalues [36]. Due to the non-vanishing moments of the distribution of $Tr[tt^\dagger]$, the transmission eigenvalues are bimodally distributed around 0 and 1 [23]. The number of open phonon channels in the diffusive coherent transport regime can be expressed as $N_{eff} \approx N \frac{l_{mfp}}{L}$. The power law decay in the diffusive regime can be interpreted as the closing of quantized channels as L increases.

When $g \approx 1$, phonon conduction enters the single-channel regime. The exponential decay of this channel's transmission eigenvalue with increasing L corresponds to the localization length, ξ. Deep in the localized regime $g \ll 1$, g is characterized by a log-normal distribution and relative fluctuations $\frac{var[\ln(g)]}{\langle \ln(g) \rangle^2} \propto L^{-1}$. Specifically, the magnitude and scaling of the fluctuations, and hence the distribution, of $\ln(g)$ only depends upon $\langle \ln(g) \rangle \approx {}^{-L}/_{\xi}$, which is conventionally referred to as single parameter scaling [12]. Our calculations corroborate the log-normal statistics, single parameter scaling, and self-averaging properties of $P[\ln(g)]$ originally demonstrated in [18].

Our work extends the statistical analysis to the transition from the many-channel diffusive transport regime to the single-channel localized transport regime. Because of the transition from Gaussian statistics to log-normal statistics, the distribution $P[g]$ should be asymmetric for $\langle g \rangle \approx 1$ [20]. Fig. 5 shows the asymmetric distribution around $P[g \approx 1]$. The transition between different statistics ultimately manifests as a kink in the probability distribution. This non-analytical behavior has been studied in quasi 1-D wires [19] described by the Dorokov-Mello-Pereyra-Kumar equation [21,37]. Although not discussed, this behavior is also present in the histograms for the 210 nm (8,0) SWNTs for ω =1020 cm^{-1} in [18].

In order to demonstrate single parameter scaling for $\langle g \rangle \approx 1$, three different disordered superlattices are tuned to have values of $\langle g \rangle$ within 1% of each other by choosing the appropriate values of L, ω, and disorder concentration. The first two configurations are superlattices with 2.38% and 4.76% ErAs interfacial density and interfacial roughness. The third configuration is a superlattice with interfacial roughness but without ErAs. The three probability distributions of Fig. 5 show excellent overlap.

$\langle g \rangle$ is thus determined to be an appropriate scaling variable [38]. The universal distribution implies that the scaling of the dimensionless conductance is independent of the ~1 nm ErAs correlation length, phonon frequency, disorder strength, and nanoparticle concentration. Furthermore, the majority of the modes should obey single parameter scaling since they lie within the bands of the superlattice without interfacial roughness or nanoparticles [39,40]. One should note, however, that the localization lengths corresponding to the configurations of Fig. 5 are ~10μm. Interfacial mixing and low nanoparticle concentrations are not a strong enough source of disorder to demonstrate the anomalous thermal conductivity maximum depicted prior.

In conclusion, the authors of this work investigated the coherent phonon transport through GaAs/AlAs superlattices with randomly embedded ErAs nanoparticles. Unlike the case of isotope disordered nanotubes, which exhibit localization at the highest phonon frequencies, the nanoparticle size and extremely large mass mismatch in our systems allows for significant localization at phonon frequencies pertinent to thermal transport. At temperatures large enough to significantly populate ~ 1.5 THz phonons, the thermal conductivity develops a local maximum as a function of length for large enough disorder concentrations. For low disorder concentrations and temperatures, the thermal conductivity monotonically increases to its asymptotic bulk value. By computing the probability distribution of the dimensionless conductance, the diffusive and localized regimes can be identified with multi-channel and single-channel transport, respectively. The transition between these two regimes is shown to occur when $\langle g \rangle \approx 1$, indicated by an asymmetric distribution and non-analytic behavior around $P[g \approx 1]$. The probability distribution is shown to depend only on $\langle g \rangle$, denoting a universal scaling behavior that is independent of the microscopic details of disorder.

This work was supported by S^3TEC, an Energy Frontier Research Center funded by the U.S. department of energy, Office of Basic Energy Sciences, under Award No. DE-FG02-09ER46577. We give thanks to J. Zhou and K. Esfarjani for their instructive discussion.

[1] D. G. Cahill, W. K. Ford, K. E. Goodson, G. D. Mahan, A. Majumdar, H. J. Maris, R. Merlin, and S. R. Phillpot, J. Appl. Phys. **93**, 793 (2003).
[2] G. Chen, *Nanoscale Energy Transport and Conversion: A Parallel Treatment of Electrons, Molecules, Phonons, and Photons*. (Oxford University Press, 2005).
[3] D. G. Cahill, P. V. Braun, G. Chen, D. R. Clarke, S. Fan, K. E. Goodson, P. Keblinski, W. P. King, G. D. Mahan, A. Majumdar, H. J. Maris, S. R. Phillpot, E. Pop, and L. Shi, Appl. Phys. Rev. **1**, (2014).
[4] M. N. Luckyanova, J. Garg, K. Esfarjani, A. Jandl, M. T. Bulsara, A. J. Schmidt, A. J. Minnich, S. Chen, M. S. Dresselhaus, Z. Ren, E. a Fitzgerald, and G. Chen, Science **338**, 936 (2012).
[5] P. W. Anderson, Phys. Rev. **109**, 1492 (1958).
[6] P. Sheng, *Introduction to Wave Scattering, Localization and Mesoscopic Phenomena* (2006).
[7] E. N. Economou, Phys. A Stat. Mech. Its Appl. **167**, 215 (1990).
[8] S. John, Phys. Rev. Lett. **58**, 2486 (1987).
[9] P. Sheng and Z. Q. Zhang, Phys. Rev. Lett. **57**, 1879 (1986).
[10] T. R. Kirkpatrick, Phys. Rev. B **31**, 5746 (1985).

[11] I. Savić, N. Mingo, and D. A. Stewart, Phys. Rev. Lett. **101**, (2008).
[12] E. Abrahams, P. W. Anderson, D. C. Licciardello, and T. V. Ramakrishnan, Phys. Rev. Lett. **42**, 673 (1979).
[13] M. Luckyanova, J. Mendoza, H. Lu, S. Huang, J. Zhou, M. Li, B. J. Kirby, A. J. Grutter, A. A. Puretzky, M. S. Dresselhaus, A. C. Gossard, and G. Chen, arXiv Prepr. arXiv1602.05057. (2015).
[14] W. Zhang, T. S. Fisher, and N. Mingo, Numer. Heat Transf. Part B Fundam. **51**, 333 (2007).
[15] A. R. Rocha, V. M. García-Suárez, S. Bailey, C. Lambert, J. Ferrer, and S. Sanvito, Phys. Rev. B - Condens. Matter Mater. Phys. **73**, (2006).
[16] M. Büttiker, Y. Imry, R. Landauer, and S. Pinhas, Phys. Rev. B **31**, 6207 (1985).
[17] P. W. Anderson, D. J. Thouless, E. Abrahams, and D. S. Fisher, Phys. Rev. B **22**, 3519 (1980).
[18] T. Yamamoto, K. Sasaoka, and S. Watanabe, Phys. Rev. Lett. **106**, (2011).
[19] K. A. Muttalib, P. Wölfle, A. García-Martín, and V. A. Gopar, EPL (Europhysics Lett. **61**, 95 (2003).
[20] P. Markoš, Acta Phys. Slovaca **56**, 561 (2006).
[21] O. N. Dorokhov, JETP Lett **36**, 318 (1982).
[22] Y. Imry, Europhys. Lett. **1**, 249 (1986).
[23] J. B. Pendry, A. MacKinnon, and P. J. Roberts, Proc. R. Soc. A Math. Phys. Eng. Sci. **437**, 67 (1992).
[24] S. Baroni, S. De Gironcoli, A. Dal Corso, and P. Giannozzi, Rev. Mod. Phys. **73**, 515 (2001).
[25] M. P. L. Sancho, J. M. L. Sancho, and J. Rubio, J. Phys. F Met. Phys. **14**, 1205 (2000).
[26] A. Amir, J. J. Krich, V. Vitelli, Y. Oreg, and Y. Imry, Phys. Rev. X **3**, (2013).
[27] S. Datta, *Electronic Transport in Mesoscopic Systems* (1995).
[28] D. J. Thouless, Phys. Rev. Lett. **39**, 1167 (1977).
[29] A. Lherbier, M. P. Persson, Y. M. Niquet, F. Triozon, and S. Roche, Phys. Rev. B - Condens. Matter Mater. Phys. **77**, (2008).
[30] C. W. J. Beenakker, Rev. Mod. Phys. **69**, 731 (1997).
[31] E. Economou, *Green's Functions in Quantum Physics*, 3rd ed. (Springer, New York, 1984).
[32] J. Mendoza, K. Esfarjani, and G. Chen, J. Appl. Phys. **117**, (2015).
[33] M. Büttiker, Phys. Rev. B **33**, 3020 (1986).
[34] P. A. Lee and A. D. Stone, Phys. Rev. Lett. **55**, 1622 (1985).
[35] D. S. Fisher and P. A. Lee, Phys. Rev. B **23**, 6851 (1981).
[36] A. Peña, A. Girschik, F. Libisch, S. Rotter, and a a Chabanov, Nat. Commun. **5**, 3488 (2014).
[37] P. A. Mello, P. Pereyra, and N. Kumar, Ann. Phys. (N. Y). **181**, 290 (1988).
[38] K. Slevin, P. Markoš, and T. Ohtsuki, Phys. Rev. Lett. **86**, 3594 (2001).
[39] L. I. Deych, A. A. Lisyansky, and B. L. Altshuler, Phys. Rev. Lett. **84**, 2678 (2000).
[40] L. I. Deych, A. A. Lisyansky, and B. L. Altshuler, Phys. Rev. B **64**, 224202 (2001).

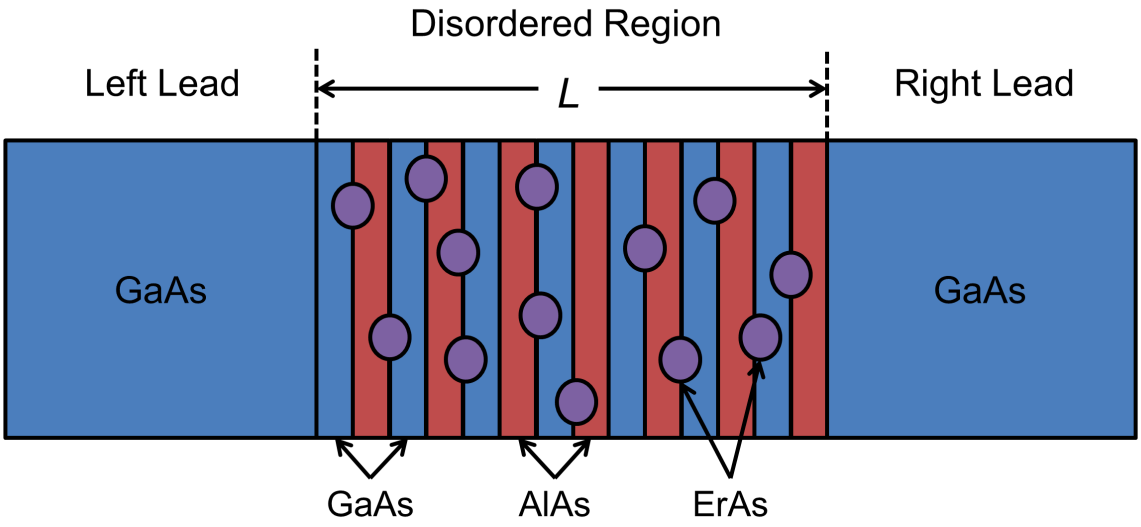

FIG. 1 Diagram of an ErAs disordered GaAs/AlAs superlattice connected to semi-infinite GaAs leads. An infinitesimal temperature difference dT establishes a net phonon flux across the disordered region.

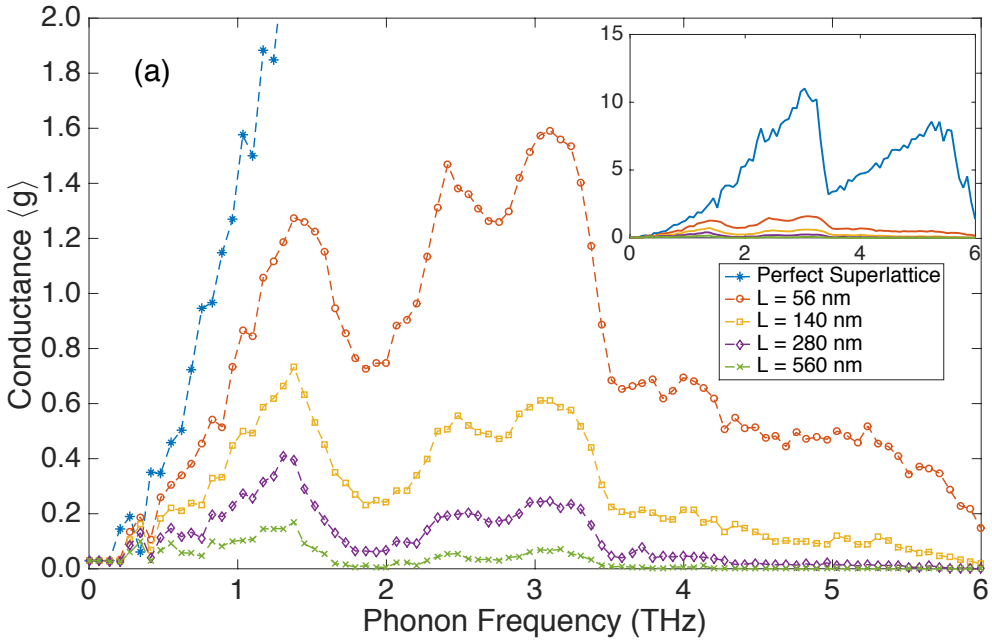

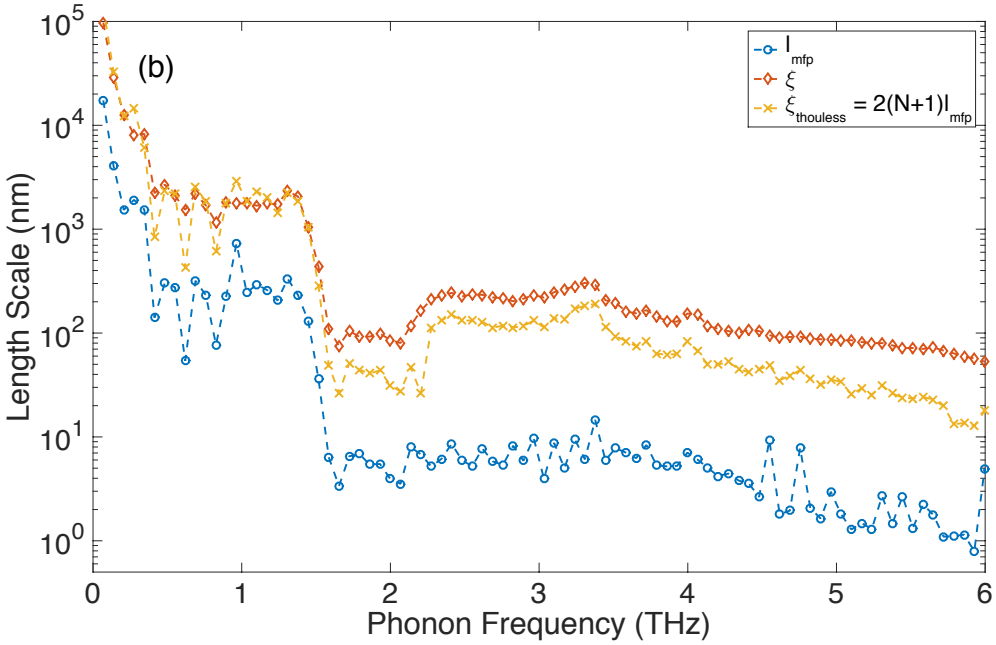

FIG. 2 (a) Configuration averaged dimensionless conductance, $\langle g \rangle$, versus phonon frequency, ω, for GaAs/AlAs superlattices with 23.8% ErAs interfacial coverage. The blue line corresponds to the dimensionless conductance of a 560 nm ordered GaAs/AlAs superlattice. 20 configurations were used for the averaging procedures for $L \geq 140$ nm while 40 configurations were used for $L = 56$ nm. Inset: Rescaled axes to show the relative difference in dimensionless conductance between the ordered and disordered superlattices. (b) The phonon mean free path (blue circles), localization length (red squares), and Thouless length (yellow crosses) versus frequency for normal incident phonons ($k_\perp = 0$). 200 configurations were computed to obtain the expected values $\langle g \rangle$ and $\langle \ln(g) \rangle$ in order to fit l_{mfp} and ξ, respectively.

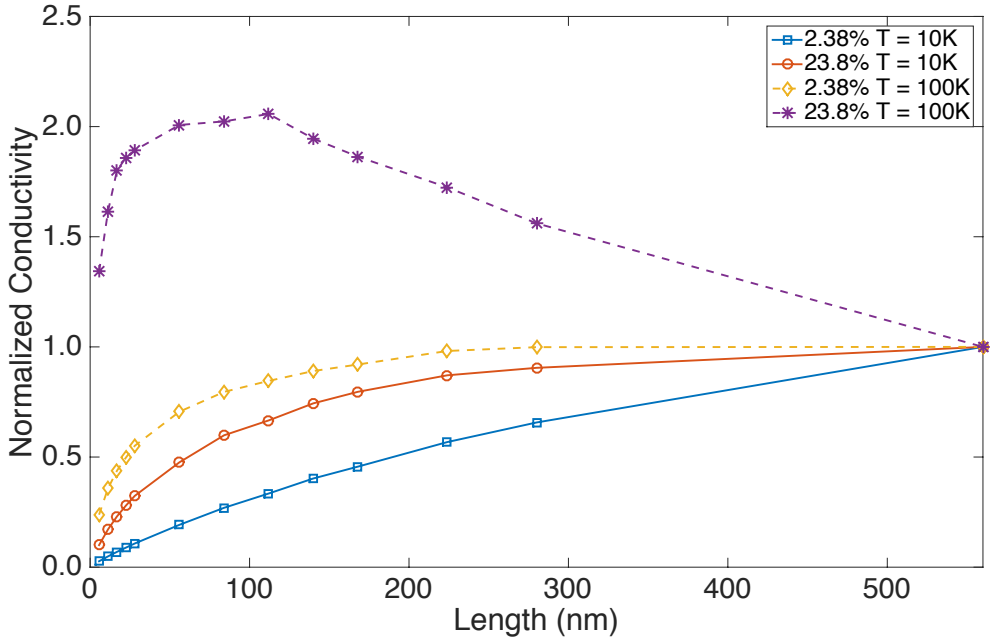

FIG. 3 Normalized thermal conductivity versus length of GaAs/AlAs superlattices with 2.38% and 23.8% ErAs interfacial coverage for T = 10K and T = 100K. Each curve is normalized by its respective value at 560 nm. Anderson localization leads to the local thermal conductivity maximum at L = 112 nm for the 23.8% interfacial disordered configurations at 100K.

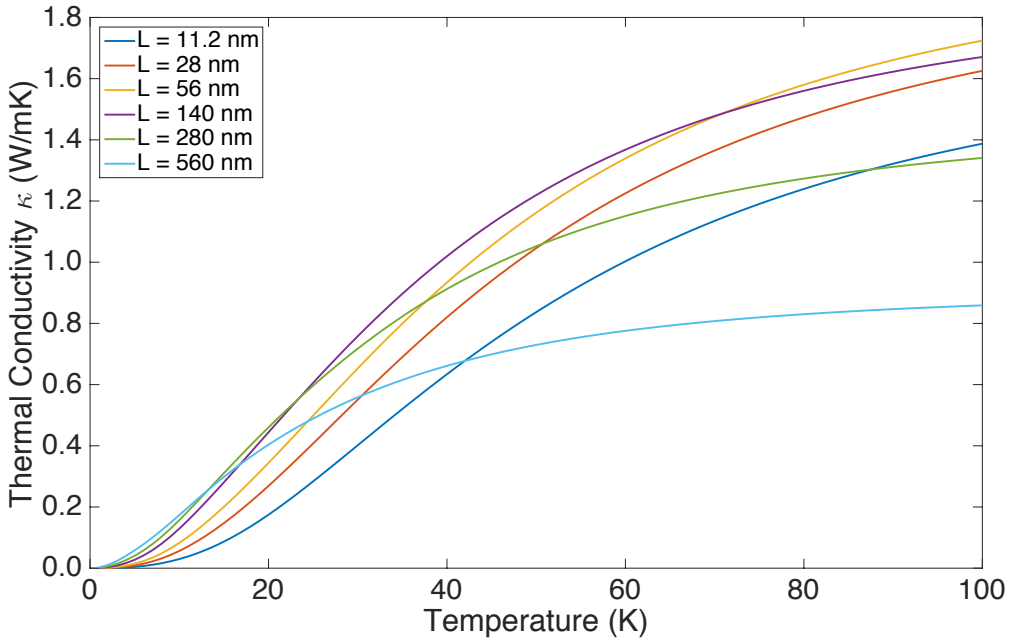

FIG. 4 Thermal conductivity versus temperature of GaAs/AlAs superlattices with 23.8% ErAs interfacial coverage for various lengths. The crossing of the curves of $\kappa(T)$ corresponds to the onset of appreciable localized phonon transport with increasing T.

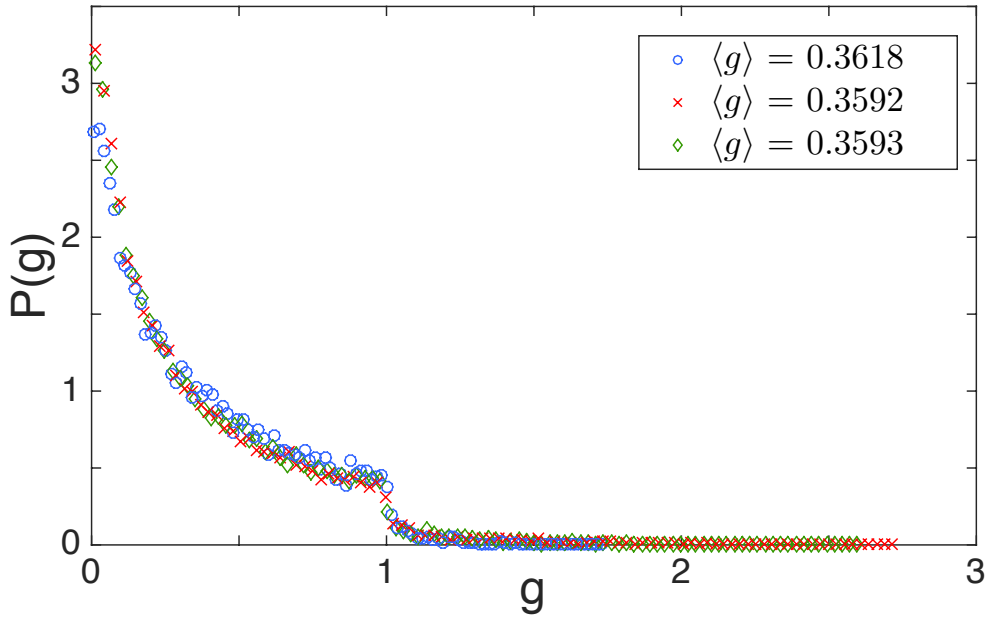

FIG. 5 Computed probability distribution of the dimensionless conductance for three different disordered superlattices. Circles correspond to superlattices with 0% ErAs, interfacial roughness, $L = 935$ nm, $\omega = 1.93$ THz, and $N = 2.1\times10^4$ configurations. Crosses correspond to superlattices with 2.38% ErAs, interfacial roughness, $L = 1120$ nm, $\omega = 1.52$ THz, and $N = 1.5\times10^4$ configurations. Diamonds correspond to superlattices with 4.76% ErAs, surface roughness, $L = 577$ nm, $\omega = 1.52$ THz, and $N = 3.2\times10^4$ configurations.